

First-Principles Study of High-Temperature Superconductivity in X_2MH_6 Compounds under 20 GPa

Jing Luo¹, Qun Wei^{1,a)}, Xiaofei Jia¹, Meiguang Zhang^{2,a)}, Xuanmin Zhu³

AFFILIATIONS

¹School of Physics, Xidian University, Xi'an 710071, China

²College of Physics and Optoelectronic Technology, Baoji University of Arts and Sciences, 721016 Baoji, China

³School of Information, Guizhou University of Finance and Economics, Guiyang 550025, China

^{a)}Authors to whom correspondence should be addressed: qunwei@xidian.edu.cn and zhmgbj@126.com.

ABSTRACT

Research on high-temperature superconductors has primarily focused on hydrogen-rich compounds, however, the need for extreme pressures limits their practical applications. The X_2MH_6 -type structure Mg_2IrH_6 stands out because it exhibits superconductivity at 160 K under ambient pressure. This study investigates methods to increase the superconducting transition temperature of this structure via atomic substitution and low-pressure treatment and assess the mechanical, thermodynamic, and dynamic stability of structures obtained by substituting Mg and Ir atoms in Mg_2IrH_6 with elements from the same groups using first-principles calculations. The findings identify 11 stable ternary compounds, 10 of which exhibit superconducting transition temperatures, with three compounds, Mg_2CoH_6 , Mg_2RhH_6 , and Mg_2IrH_6 , exceeding 100 K, classifying them as high-temperature superconductors. Their superconducting figure of merit S values are 2.71, 3.35, and 3.83, respectively, suggesting strong practical application potential. The analysis results indicate that mid-frequency hydrogen phonons significantly enhance superconducting properties via electron-

phonon coupling. The band structure study highlights the importance of van Hove singularities near the Fermi level. In addition, electron localization function and Fermi surface topology analyses reveal that the Fermi surface shape and density of states are crucial for increasing superconducting transition temperatures.

Since mercury was discovered to exhibit zero resistance at 4.2 K, research into superconductivity in condensed matter physics has advanced rapidly. By exploring the microscopic mechanisms of superconductivity, the Bardeen-Cooper-Schrieffer theory¹ was developed to explain superconducting behavior at low temperatures. However, the critical temperature of most currently synthesized superconductors remains below the temperature of liquid nitrogen (77 K), thus, research on high-temperature superconductors is essential. Based on advanced crystal structure search methods²⁻⁶, many hydrogen-rich compounds⁷⁻⁹ under high pressure have been predicted to exhibit high critical temperatures. Among them, H₃S¹⁰, LaH₁₀¹¹⁻¹², and YH₆¹³ have been experimentally confirmed to have critical temperatures above 200 K under high pressure, whereas Li₂MgH₁₆¹⁴, Li₂NaH₁₇¹⁵, and Li₂Na₃H₂₃¹⁵ have been predicted to exhibit room-temperature superconductivity under pressure. Research on hydrogen-rich compounds indicates that superconducting critical temperatures close to room temperature can be achieved through the conventional mechanism of electron-phonon interactions¹⁶⁻¹⁷. However, superconductors with excellent superconducting properties typically require a minimum stable pressure of 150 GPa¹⁷. This condition significantly limits the practical applications of these materials.

Notably, the Mg₂IrH₆ structure proposed by Dolui et al. exhibits a superconducting transition temperature (160 K) under ambient pressure¹⁸. To further enhance the transition temperature of this structure, we performed atomic substitution and applied additional pressure based on the structure. Based on the ternary convex hull provided by Dolui¹⁸, Mg₂IrH₆ is thermodynamically stable at 20 GPa; therefore, we applied a pressure of 20 GPa to this structure. Here, atomic substitution was used to replace the Mg and Ir atoms in Mg₂IrH₆ with elements from the second and ninth groups at 20 GPa. By evaluating the mechanical, thermodynamic, and dynamic stability of the resulting

structures, we identified 11 stable configurations. After excluding the non-metallic components from these stable structures, we conducted in-depth analysis of the electrical and superconducting properties of the 10 obtained metallic structures to provide insights into the design of superconductors at room temperature and ambient pressure.

The Vienna Ab initio Simulation Package (VASP) was used to perform relaxation and simulate the related properties of the 15 substituted structures¹⁹. The projector-augmented wave potentials²⁰ and Perdew–Burke–Ernzerhof exchange–correlation functional under generalized gradient approximation²¹ were adopted. A cut-off energy of 400 eV was applied for plane wave expansion, and the Monkhorst–Pack k -grid²² with a spacing of $2\pi \times 0.02 \text{ \AA}^{-1}$ was used to ensure adequate convergence ($1 \times 10^{-5} \text{ eV/atom}$) of the total energy. In addition, the single-crystal elastic constants were determined from the strain–stress relationships derived by applying six finite deformations²³. Dynamic stability was evaluated via the finite displacement approach, with phonon spectra computed using the PHONOPY package²⁴. Electron–phonon coupling (EPC) was analyzed using Quantum ESPRESSO²⁵, with kinetic energy cut-offs set at 50 Ry, and ultrasoft pseudopotentials were applied. A $16 \times 16 \times 16$ k -grid was used to determine the self-consistent electron density, and a $4 \times 4 \times 4$ q -grid was employed to calculate the EPC constant. The superconducting critical temperatures (T_c) value was calculated using the Allen-Dynes modified McMillan equation²⁶.

The X_2MH_6 structure is a face-centred cubic phase characterized by the MH_6 octahedral structural unit, where X represents Be, Mg, Ca, Sr, and Ba atoms, and M represents Co, Rh, and Ir atoms (Fig. 1). Ten stable ternary metal structures were identified. The specific process involves first calculating the elastic constants of these structures, followed by evaluating their mechanical stability according to the Born criteria²⁷, excluding those that do not meet the Born criteria. The elastic constants of the ten structures were listed in Table S1 in the supplementary material. For mechanically stable structures, the formation energy is used to evaluate their thermodynamic stability, which can be calculated using the following formula:

$$\Delta H = [E(X_2MH_6) - 2E(X) - E(M) - 6E(H)]/9 \quad (1)$$

where ΔH denotes the formation energy of a material; $E(X_2MH_6)$ denotes the total energy of the structure and $E(X)$, $E(M)$ and $E(H)$ denote the average energies of X, M, and H atom, respectively. After obtaining 12 thermodynamically and mechanically stable structures, their dynamical stability was assessed by calculating their phonon spectra to check for the presence of imaginary frequencies below zero. This process ultimately identified 11 stable structures. Finally, 10 stable metallic structures were identified by calculating their band gaps. The detailed screening results are presented in Fig. 1(b). The ten stable metallic structures were as follows: Mg_2CoH_6 , Mg_2RhH_6 , Mg_2IrH_6 , Ca_2CoH_6 , Ca_2RhH_6 , Ca_2IrH_6 , Sr_2CoH_6 , Sr_2IrH_6 , Ba_2RhH_6 , and Ba_2IrH_6 .

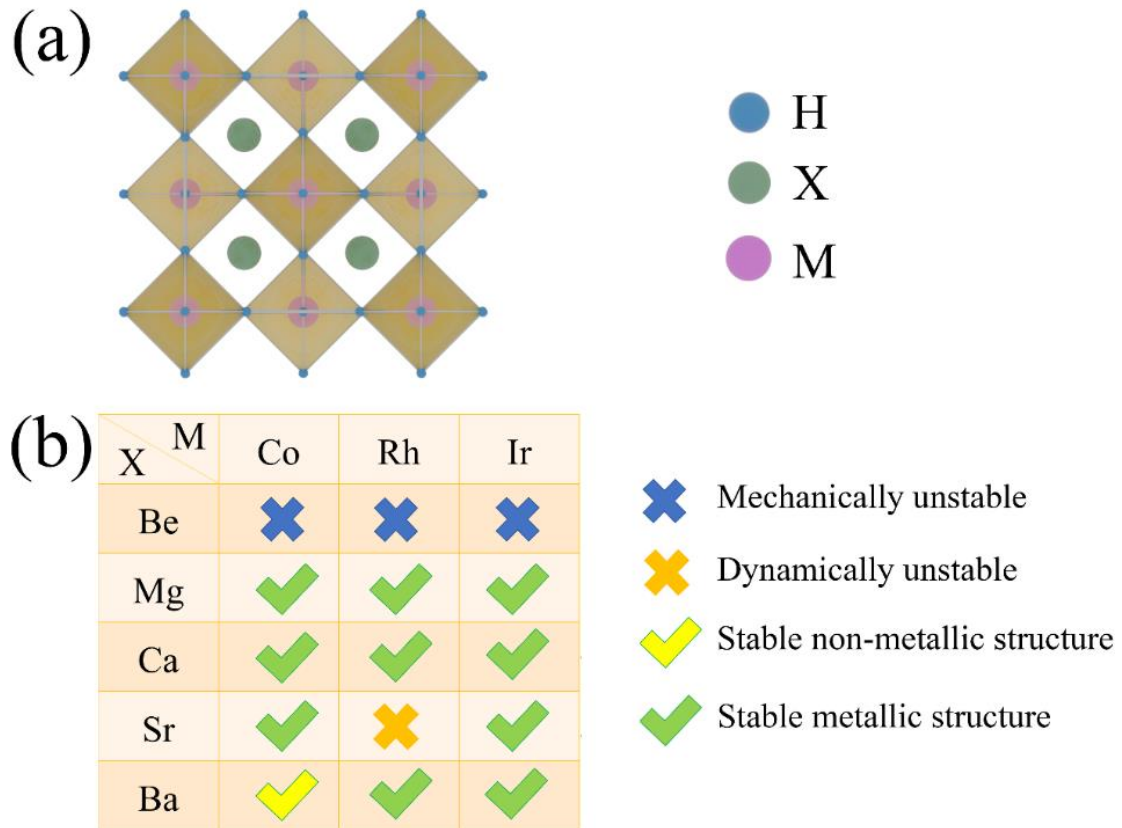


Fig. 1. (a) Prototype structure of X_2MH_6 . The X, M, and H atoms are coloured in green, red and blue, respectively. (b) Screening results.

TABLE I. EPC constant λ , logarithmic average phonon frequency ω_{\log} (in K), density of states at the Fermi level N_F (in eV^{-1}), superconducting figure of merit S and superconducting transition temperature T_c (in K) of the structures under pressure.

Structures	Pressure (GPa)	λ	ω_{\log} (K)	N_F (eV^{-1})	T_c (K)	S
Mg ₂ IrH ₆	20	3.04	927.52	64.74	167.8	3.83
Mg ₂ IrH ₆ ²⁸	0				77.0	1.94
Mg ₂ RhH ₆	20	2.05	1002.21	43.89	146.8	3.35
Mg ₂ RhH ₆ ²⁸	0				48.5	1.24
Mg ₂ CoH ₆	20	1.34	1169.38	53.89	118.5	2.71
Ca ₂ IrH ₆	20	0.68	1372.79	38.09	44.3	1.01
Ca ₂ RhH ₆	20	0.51	849.56	32.72	11.4	0.26
Ca ₂ CoH ₆	20	0.39	1454.86	38.75	4.9	0.11
Sr ₂ IrH ₆	20	0.43	429.14	28.32	2.7	0.06
Sr ₂ CoH ₆	20	0.27	641.45	34.15	0.1	0.002
Ba ₂ RhH ₆	20	0.62	329.59	29.05	8.4	0.19
Ba ₂ IrH ₆	20	0.27	1077.48	26.11	0.1	0.003

After identifying the stable structures, we used Quantum ESPRESSO to calculate the superconducting transition temperatures of the ten structures. The results are presented in Table I. The transition temperature of the structures are expressed using the Allen-Dynes modified McMillan equation²⁶:

$$T_c = \frac{\omega_{\log}}{1.20 \exp \left[-\frac{1.04(1 + \lambda)}{\lambda(1 - 0.62\mu^*)} \right]} \quad (2)$$

where ω_{\log} denotes the logarithmic average phonon frequency, λ denotes the EPC constant and μ^* denotes the Coulomb potential parameter. λ can be determined by integrating the Eliashberg spectral function $\alpha^2F(\omega)$ in the frequency space:

$$\lambda = 2 \int \frac{\alpha^2F(\omega)}{\omega d\omega} \quad (3)$$

Fig. 2 shows the Eliashberg phonon spectral function $\alpha^2F(\omega)$ and λ . We set μ^* to 0.1. The calculated λ and ω_{\log} , along with the calculated T_c values, presented in Table

I. The superconducting transition temperatures of Mg_2IrH_6 and Mg_2RhH_6 at 0 GPa²⁸ are also presented in Table I. A comparison reveals that applying 20 GPa of pressure increases the transition temperatures of these structures. Among the ten X_2MH_6 structures, the superconducting transition temperatures of the Mg_2MH_6 structures (M = Ir, Rh, Co) exceed 100 K, thereby classifying them as high-temperature superconductors. In contrast, when X is Ca, Sr, or Ba, the transition temperatures fall below 77 K, rendering these structures of limited practical value. To enhance their transition temperatures, the applied pressure may be increased further. The superconducting figure of merit S is used to comprehensively evaluate the performance and practicality of superconducting materials²⁹. This metric not only considers the superconducting transition temperature T_c but also incorporates the pressure conditions, reflecting the feasibility of superconducting materials in real-world applications. MgB_2 , as a material with technological applications, has a superconducting figure of merit of $S = 1$. In contrast, the S values of the high-temperature superconducting structures we calculated in this study range from 2.71 to 3.83, which are higher than that of MgB_2 , indicating that these structures have greater potential for practical applications. The superconducting figures of merit for all structures are presented in Table I.

EPC is a key factor influencing the superconducting transition temperature of superconductors. As shown in Fig. 2, the EPC values of the ten structures are primarily contributed by phonons in three frequency ranges: low-frequency modes (<15 THz), mid frequency-modes (15–40 THz), and high-frequency modes (>40 THz). For the high-temperature superconductors Mg_2CoH_6 , Mg_2RhH_6 , and Mg_2IrH_6 , the contributions of low-frequency modes to the EPC constant were 27.1%, 23.6%, and 22.4%, respectively. The contributions of mid-frequency modes were 49.1%, 47.3%, and 51.8%, respectively, whereas the contributions of high-frequency modes were 23.8%, 29.1%, and 25.8%, respectively. For the low-temperature superconductors Ca_2IrH_6 , Ca_2RhH_6 , Ca_2CoH_6 , Sr_2IrH_6 , Sr_2CoH_6 , Ba_2RhH_6 , and Ba_2IrH_6 , the contributions of low-frequency modes to the EPC constant were 22.1%, 41.2%, 20.5%, 62.8%, 55.6%, 58.1%, and 28.6%, respectively. The contributions of mid-frequency modes were 32.3%, 33.3%, 5.1%, 20.9%, 18.5%, 12.9%, and 1.1%, respectively. In

contrast, the contributions of high-frequency modes were 45.6%, 25.5%, 74.4%, 16.3%, 25.9%, 29.0%, and 70.3%, respectively. In high-temperature superconductors, phonons in the mid-frequency range contribute more significantly to the EPC constant, whereas the influence of high-frequency and low-frequency phonons on EPC is roughly comparable. In contrast, in low-temperature superconductors, the contribution of mid-frequency phonons is relatively smaller, with the highest contribution being only 33.3% and the lowest as little as 1.1%. In contrast, the contributions of high- and low-frequency phonons exhibit considerable variation.

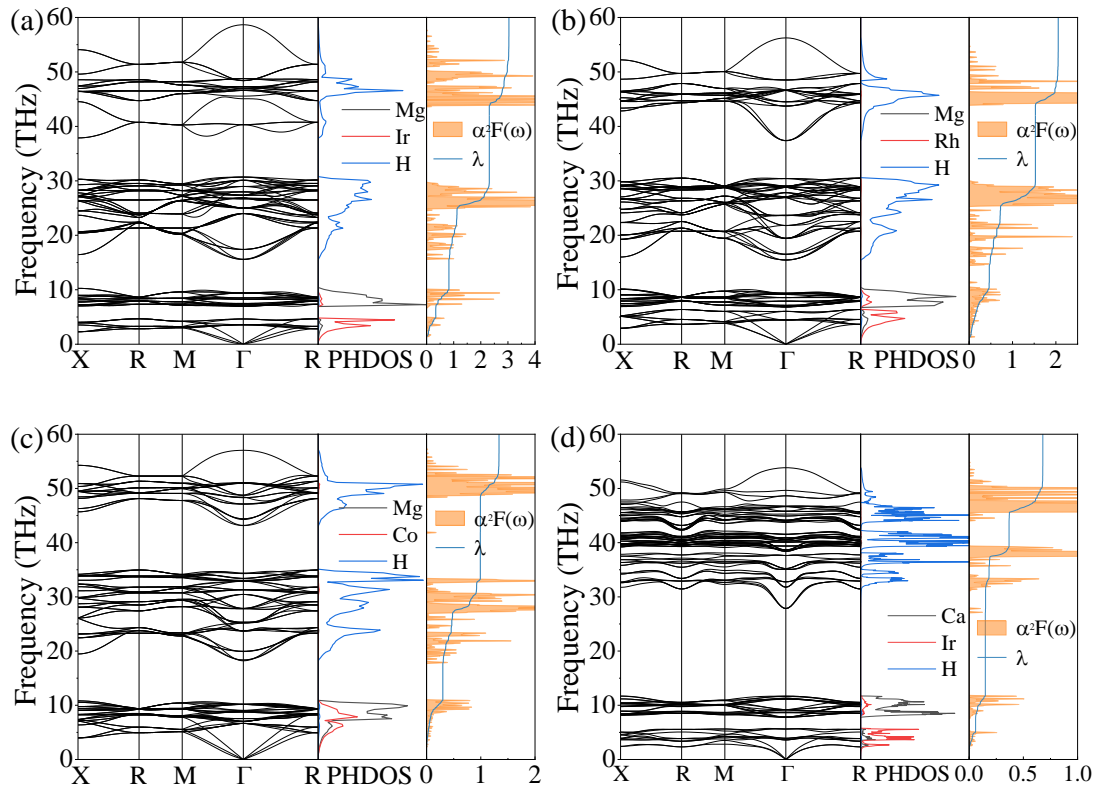


FIG. 2. Calculated phonon dispersion curves, phonon density of states, Eliashberg phonon spectral function $\alpha^2F(\omega)$, and EPC parameter λ of the (a) Mg_2IrH_6 , (b) Mg_2RhH_6 , (c) Mg_2CoH_6 , (d) Ca_2IrH_6 . (The phonon spectrums of the other six structures are provided in the Fig. S1 in the supplementary material.)

To further investigate the relationship between atoms and phonons, the phonon dispersion curves and phonon density of states of the obtained structures are presented in Figs. 2 and S1. The figures show that the low-frequency phonons are primarily

contributed by the two metallic elements, whereas the mid- and high-frequency phonons are primarily contributed by hydrogen atoms. Therefore, for high-temperature superconductors, mid-frequency hydrogen atoms predominantly contribute to EPC, thereby increasing the superconducting transition temperature. In contrast, for low-temperature superconductors, the contributions from metal atoms and high-frequency hydrogen atoms to the EPC are more significant, while the absence of mid-frequency phonons may limit the enhancement of the superconducting transition temperature.

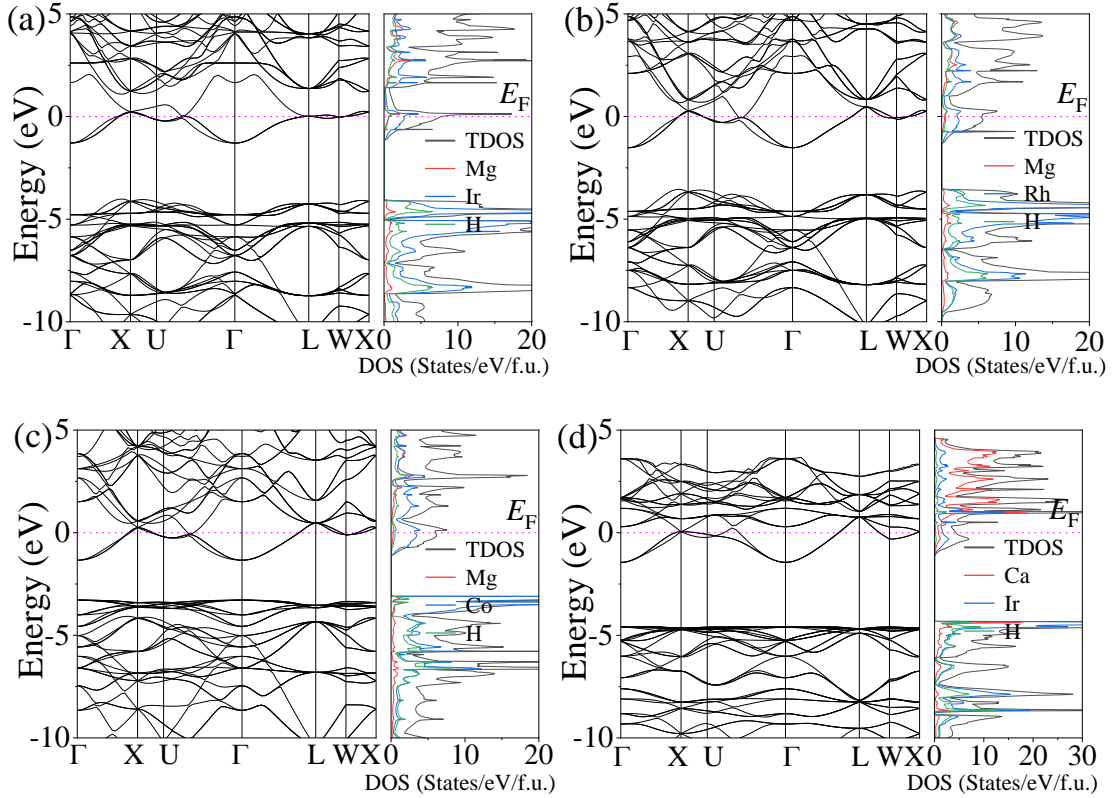


FIG. 3. Calculated band structures and the density of states of the (a) Mg_2IrH_6 , (b) Mg_2RhH_6 , (c) Mg_2CoH_6 , (d) Ca_2IrH_6 (The band structures and the density of states of the other six structures are provided in Fig. S2 in the supplementary material.)

The electronic structure of materials is closely related to their superconductivity. Thus, the band structures and density of states of the obtained structures are plotted in Figs. 3 and S2. The electronic structure of the high-temperature superconductors exhibits distinctive features near the Fermi level. For example, the Mg_2IrH_6 structure exhibits a van Hove singularity near the Fermi level, characterized by an energy peak,

which could explain its highest superconducting transition temperature. In contrast, the lower transition temperatures of Mg_2RhH_6 and Mg_2CoH_6 may be due to the presence of van Hove singularities near the Fermi level but with energy valleys instead of peaks. Compared to high-temperature superconductors, the van Hove singularity in low-temperature superconductors is farther from the Fermi level; thus, it does not significantly increase the density of states at the Fermi level. This may explain the lower superconducting transition temperatures of these structures.

In addition, the difference between high- and low-temperature superconductors lies in the contribution of hydrogen atoms at the Fermi level. The hydrogen content at the Fermi level is a significant factor in increasing the superconducting transition temperature³⁰. According to the density of state shown in Fig. 3, in all structures, the Fermi level is primarily dominated by M atoms. However, in the high-temperature superconducting structures, the contribution of H atoms is greater than or equal to that of X atoms, whereas, in the low-temperature superconductors, the contribution of H atoms is lower and significantly less than that of X atoms.

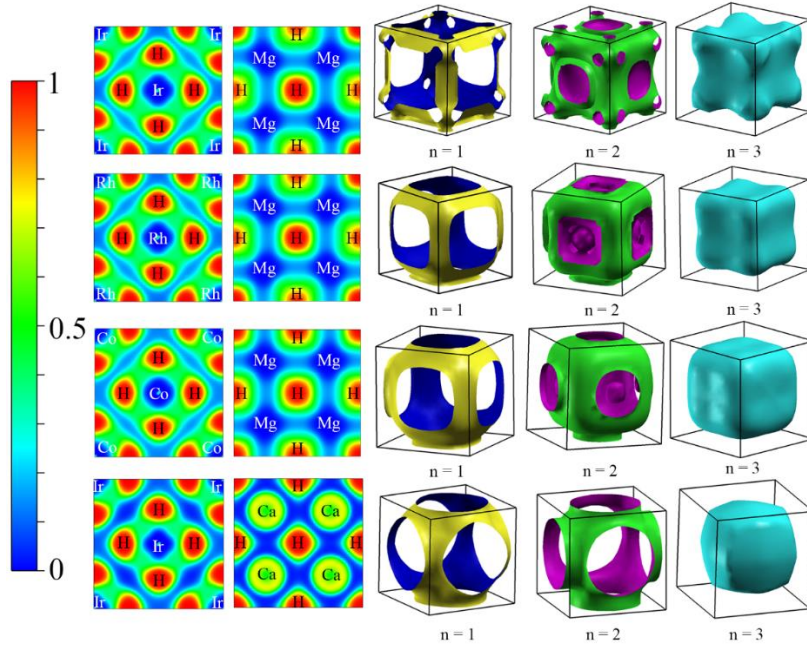


FIG. 4. Electronic localization function (ELF) and Fermi surface topology of superconductors. (The ELF and Fermi surface topology of the other six structures are provided in Fig. S3 in the supplementary material.)

To explore additional factors affecting the transition temperature, we plotted the ELF and Fermi surface topologies of these structures. Fig. 4 and S3 present the ELF and Fermi surfaces of the 10 superconductors. The ELF plots of these structures show a minimal overlap of electron clouds between metal atoms and between metal and H atoms, indicating the absence of strong interactions between them. In contrast, the ELF values between H atoms are approximately 0.5, suggesting that some H atoms form weak covalent bonds. According to our calculations, the covalent bond length between hydrogen bonds (H–H) is 2.418 Å. Based on the structure diagram of X_2MH_6 , it can be determined that the H atoms form an octahedral hydrogen cage with a length of 2.418 Å, enclosing the M atom.

Comparing the ELF maps between the X and H atoms, the larger red region surrounding the H atom in the high-temperature superconductor indicates stronger electron localization, which promotes the formation of Cooper pairs, thereby enhancing EPC and increasing the superconducting transition temperature. In contrast, the green region surrounding the X atom in the low-temperature superconductor suggests an increase in electron delocalization, resulting in a reduction in the EPC strength.

The superconducting properties of these structures are closely related to the topology of the Fermi surface. At $n = 1$, the Fermi surfaces of all structures exhibit an open centre and closed edges, indicating that there may be numerous open orbits in the Brillouin zone, with minimal restriction on electron movement, leading to improved electronic conductivity. At $n = 3$, the Fermi surfaces of all structures display a closed and smoother shape, indicating that the structures exhibit typical metallic characteristics. However, at $n = 2$, the Fermi surface topology differs significantly between the high- and low-temperature superconductors. The Fermi surface of low-temperature superconductors at $n = 2$ is similar to that at $n = 1$, whereas the Fermi surface of the high-temperature superconductors is significantly more complex, featuring multilayered structures and closed shapes. This likely suggests that the electron distribution is more intricate, with stronger orbital overlap, resulting in an increased density of states near the Fermi level. In general, a higher density of states near the Fermi surface favours the formation of Cooper pairs, which enhances EPC and

increases the superconducting transition temperature.

In summary, to enhance the superconducting transition temperature of high-temperature superconductor Mg_2IrH_6 , we combined atomic substitution and applied a pressure of 20 GPa, yielding 15 ternary structures. By substituting metal atoms from Groups II and IX and screening based on formation energy, the Born criterion, and phonon stability, we identified 11 stable structures, 10 of which exhibit metallic properties. The superconducting transition temperatures of the high-temperature superconductors Mg_2IrH_6 , Mg_2RhH_6 , and Mg_2CoH_6 reached 167.8 K, 146.76 K, and 118.51 K, respectively, whereas the transition temperatures of the remaining structures were all below 77 K. Our study found that mid-frequency phonons (15-40 THz), particularly those associated with hydrogen, significantly affect EPC, thereby increasing the transition temperature. In addition, the band structure and ELF analyses revealed that the proximity of the van Hove singularity to the Fermi level and the contribution of hydrogen atoms at the Fermi level are key factors influencing superconducting performance. Furthermore, the complex multilayered topology of the Fermi surface increases the density of states, further increasing the superconducting transition temperature.

See the supplementary material for Figs. S1–S3 and Tables S1.

This work was financially supported by the National Natural Science Foundation of China (Grant Nos.: 11965005 and 11964026), the Natural Science Basic Research plan in Shaanxi Province of China (Grant Nos.: 2023-JC-YB-021, 2022JM-035), the Fundamental Research Funds for the Central Universities, and the 111 Project (B17035). All the authors thank the computing facilities at High Performance Computing Center of Xidian University.

AUTHOR DECLARATIONS

Conflict of Interest

The authors have no conflicts to disclose.

Author Contributions

Jing Luo: Investigation, Data curation, Writing – original draft. **Qun Wei:** Supervision, Project administration, Writing – review & editing. **Xiaofei Jia:** Investigation, Data curation. **Meiguang Zhang:** Resources, Funding acquisition. Writing – review & editing. **Xuanmin Zhu:** Investigation.

DATA AVAILABILITY

The data that support the findings of this study are available from the corresponding author upon reasonable request.

REFERENCES

- ¹L. N. Cooper, J Bardeen, and J. R. Schrieffer, Phys. Rev. **108**, 1175 (1957).
<https://doi.org/10.1119/1.1935097>
- ²S. Q. Wu, M. Ji, C. Z. Wang, M. C. Nguyen, X. Zhao, K. Umemoto, R. M. Wentzcovitch, and K. M. Ho, J. Phys.: Condens.Matter **26**(3), 035402 (2014).
<http://dx.doi.org/10.1088/0953-8984/26/3/035402>
- ³Y. Wang, J. Lv, L. Zhu, and Y. Ma, Comput. Phys. Commun. **183**(10), 2063 (2012).
<http://dx.doi.org/10.1016/j.cpc.2012.05.008>
- ⁴W. E. Pickett, Rev. Mod. Phys. **95**(2), 021001 (2023).
<http://dx.doi.org/10.1103/RevModPhys.95.021001>
- ⁵J. Wang, H. Gao, Y. Han, C. Ding, S. Pan, Y. Wang, Q. Jia, H. T. Wang, D.Xing, and J. Sun, Natl. Sci. Rev. **10**(7), nwad128 (2023). <http://dx.doi.org/10.1093/nsr/nwad128>
- ⁶S. Saha, S. D. Cataldo, F. Giannessi, A. Cucciari, W. von der Linden, and L. Boeri, Phys. Rev. Mater. **7**(5), 054806 (2023).
<http://dx.doi.org/10.1103/PhysRevMaterials.7.054806>
- ⁷F. Peng, Y. Sun, C. J. Pickard, R. J. Needs, Q. Wu, and Y. Ma, Phys. Rev. Lett. **119**(10), 107001 (2017). <http://dx.doi.org/10.1103/PhysRevLett.119.107001>

- ⁸H. Liu, Naumov, II. R. Hoffmann, N. W. Ashcroft, and R. J. Hemley, *Proc. Natl. Acad. Sci.* **114**(27), 6990 (2017). <http://dx.doi.org/10.1073/pnas.1704505114>
- ⁹D. Duan, Y. Liu, F. Tian, D. Li, X. Huang, Z. Zhao, H. Yu, B. Liu, W. Tian, and T. Cui, *Sci. Rep.* **4**(1), 6968 (2014). <https://doi.org/10.1038/srep06968>
- ¹⁰A. P. Drozdov, M. I. Eremets, I. A. Troyan, V. Ksenofontov, and S. I. Shylin, *Nature* **525**(7567), 73-76 (2015). <http://dx.doi.org/10.1038/nature14964>
- ¹¹A. P. Drozdov, P. P. Kong, V. S. Minkov, S. P. Besedin, M. A. Kuzovnikov, S. Mozaffari, L. Balicas, F. F. Balakirev, D. E. Graf, V. B. Prakapenka, E. Greenberg, D. A. Knyazev, M. Tkacz, and M. I. Eremets, *Nature* **569**(7757), 528-531 (2019). <http://dx.doi.org/10.1038/s41586-019-1201-8>
- ¹²M. Somayazulu, M. Ahart, A. K. Mishra, Z. M. Geballe, M. Baldini, Y. Meng, V. V. Struzhkin, and R. J. Hemley, *Phys. Rev. Lett.* **122**(2), 027001 (2019). <http://dx.doi.org/10.1103/PhysRevLett.122.027001>
- ¹³P. Kong, V. S. Minkov, M. A. Kuzovnikov, A. P. Drozdov, S. P. Besedin, S. Mozaffari, L. Balicas, F. F. Balakirev, V. B. Prakapenka, S. Chariton, D. A. Knyazev, E. Greenberg, and M. I. Eremets, *Nat. Commun.* **12**(1), 5075 (2021). <http://dx.doi.org/10.1038/s41467-021-25372-2>
- ¹⁴Y. Sun, J. Lv, Y. Xie, H. Liu, and Y. Ma, *Phys. Rev. Lett.* **123**(9), 097001 (2019). <http://dx.doi.org/10.1103/PhysRevLett.123.097001>
- ¹⁵D. An, D. Duan, Z. Zhang, Q. Jiang, H. Song, and T. Cui, arXiv preprint arXiv:2303.09805 (2023). <https://doi.org/10.48550/arXiv.2303.09805>
- ¹⁶L. Boeri and G. B. Bachelet, *J. Phys. Condens. Matter.* **31**(23), 234002 (2019). <http://dx.doi.org/10.1088/1361-648X/ab0db2>
- ¹⁷J. A. Flores-Livas, L. Boeri, A. Sanna, G. Profeta, R. Arita, and M. Eremets, *Physics Reports.* **856**, 1-78 (2020). <http://dx.doi.org/10.1016/j.physrep.2020.02.003>
- ¹⁸K. Dolui, L. J. Conway, C. Heil, T. A. Strobel, R. P. Prasankumar, and C. J. Pickard, *Phys. Rev. Lett.* **132**(16), 166001 (2024). <http://dx.doi.org/10.1103/PhysRevLett.132.166001>
- ¹⁹G. Kresse and J. Furthmüller, *Phys. Rev. B* **54**(16), 11169 (1996). <https://doi.org/10.1103/PhysRevB.54.11169>

- ²⁰G. Kresse and D. Joubert, Phys. Rev. B **59**(3), 1758 (1999).
<https://doi.org/10.1103/PhysRevB.59.1758>
- ²¹J. P. Perdew, K. Burke, and M. Ernzerhof, Phys. Rev. Lett. **77**(18), 3865 (1996).
<https://doi.org/10.1103/PhysRevLett.77.3865>
- ²²H. J. Monkhorst and J. D. Pack, Phys. Rev. B **13**(12), 5188 (1976).
<http://dx.doi.org/10.1103/PhysRevB.13.5188>
- ²³Z. Cui, Y. Sun, J. Li, and J. Qu, Phys. Rev. B **75**(21) (2007).
<http://dx.doi.org/10.1103/PhysRevB.75.214101>
- ²⁴A. Togo and I. Tanaka, Scr. Mater. **108**, 1-5 (2015).
<http://dx.doi.org/10.1016/j.scriptamat.2015.07.021>
- ²⁵P. Giannozzi, S. Baroni, N. Bonini, M. Calandra, R. Car, C. Cavazzoni, D. Ceresoli, G. L. Chiarotti, M. Cococcioni, I. Dabo, A. Dal Corso, S. de Gironcoli, S. Fabris, G. Fratesi, R. Gebauer, U. Gerstmann, C. Gougoussis, A. Kokalj, M. Lazzeri, L. Martin-Samos, N. Marzari, F. Mauri, R. Mazzarello, S. Paolini, A. Pasquarello, L. Paulatto, C. Sbraccia, S. Scandolo, G. Sclauzero, A. P. Seitsonen, A. Smogunov, P. Umari, and R. M. Wentzcovitch, J. Phys. Condens. Matter. **21**(39), 395502 (2009).
<http://dx.doi.org/10.1088/0953-8984/21/39/395502>
- ²⁶P. B. Allen and R. C. Dynes, Phys. Rev. B **12**(3), 905 (1975).
<http://dx.doi.org/10.1103/PhysRevB.12.905>
- ²⁷F. Mouhat and F. Coudert, Phys. Rev. B **90**(22), 22104 (2014).
<http://dx.doi.org/10.1103/PhysRevB.90.224104>
- ²⁸A. Sanna, T. F. T. Cerqueira, Y. W. Fang, I. Errea, A. Ludwig, and M. A. L. Marques, npj Comput. Mater. **10**, 44 (2024). <http://dx.doi.org/10.1038/s41524-024-01214-9>
- ²⁹C. J. Pickard, I. Errea, and M. I. Eremets, Annu. Rev. Condens. Matter Phys. **11**(1), 57-76 (2020). <http://dx.doi.org/10.1146/annurev-conmatphys-031218-013413>
- ³⁰F. Belli, T. Novoa, J. Contreras-Garcia, and I. Errea, Nat. Commun. **12**(1), 5381 (2021). <http://dx.doi.org/10.1038/s41467-021-25687-0>